Limnol. Oceanogr., 51(3), 2006, 1262–1273

Prokaryotic respiration and production in the meso- and bathypelagic realm of the eastern and western North Atlantic basin

Thomas Reinthaler[1]
Department of Biological Oceanography, Royal Netherlands Institute for Sea Research (NIOZ), P.O. Box 59, 1790AB Den Burg, Texel, The Netherlands

Hendrik van Aken and Cornelis Veth
Department of Physical Oceanography, Royal Netherlands Institute for Sea Research (NIOZ), P.O. Box 59, 1790AB Den Burg, Texel, The Netherlands

Javier Arístegui
Campus Universitario de Tafira, Facultad de Ciencias del Mar, Universidad de Las Palmas de Gran Canaria, 35017 Las Palmas, Spain

Carol Robinson
Plymouth Marine Laboratory, Prospect Place, West Hoe, Plymouth, Devon, PL13DH, United Kingdom

Peter J. le B. Williams
School of Ocean Sciences, University of Wales at Bangor, Menai Bridge, Anglesey, LL59AB, United Kingdom

Philippe Lebaron
Observatoire Océanologique, Laboratoire d'Océanologie Biologique de Banyuls, Université Paris VI. CNRS UMR 7621, BP44, F-66651 Banyuls-sur-Mer, France

Gerhard J. Herndl
Department of Biological Oceanography, Royal Netherlands Institute for Sea Research (NIOZ), P.O. Box 59, 1790AB Den Burg, Texel, The Netherlands

Abstract

We measured prokaryotic production and respiration in the major water masses of the North Atlantic down to a depth of ~4,000 m by following the progression of the two branches of North Atlantic Deep Water (NADW) in the oceanic conveyor belt. Prokaryotic abundance decreased exponentially with depth from 3 to 0.4×10^5 cells mL^{-1} in the eastern basin and from 3.6 to 0.3×10^5 cells mL^{-1} in the western basin. Prokaryotic production measured via ^{3}H-leucine incorporation showed a similar pattern to that of prokaryotic abundance and decreased with depth from 9.2 to 1.1 μmol C m^{-3} d^{-1} in the eastern and from 20.6 to 1.2 μmol C m^{-3} d^{-1} in the western basin. Prokaryotic respiration, measured via oxygen consumption, ranged from about 300 to 60 μmol C m^{-3} d^{-1} from ~100 m depth to the NADW. Prokaryotic growth efficiencies of ~2% in the deep waters (depth range 1,200–4,000 m) indicate that the prokaryotic carbon demand exceeds dissolved organic matter input and surface primary production by 2 orders of magnitude. Cell-specific prokaryotic production was rather constant throughout the water column, ranging from 15 to 32×10^{-3} fmol C $cell^{-1}$ d^{-1} in the eastern and from 35 to 58×10^{-3} fmol C $cell^{-1}$ d^{-1} in the western basin. Along with increasing cell-specific respiration towards the deep water masses and the relatively short turnover time of the prokaryotic community in the dark ocean (34–54 d), prokaryotic activity in the meso- and bathypelagic North Atlantic might be higher than previously assumed.

[1] Corresponding author (thomas.reinthaler@nioz.nl).

Acknowledgments

We thank the captain and crew of the R/V *Pelagia* for their support at sea. Special thanks go to Denise Cummings for help with the respiration measurements during TRANSAT-II and to Geraldine Kramer for providing the TOC data during TRANSAT-I. Santiago Gonzalez performed the TOC measurements and Philippe Catala the flow cytometry analyses. We also thank Jesús Maria Arrieta for invaluable discussions during data analysis. Toshi Nagata is acknowledged for providing his raw data on prokaryotic production of the Pacific.

C.R., P.J.leB.W., and J.A. were supported by a UK Natural Environment Research Council grant NER/B/S/2001/00846 awarded to C.R. and P.J.leB.W. C.R. was also supported by the Plymouth Marine Laboratory Core Strategic Research program. The TRANSAT cruises were supported by the Dutch Science Foundation (NWO-ALW), project 811.33.004 to G.J.H.

This work is in partial fulfillment of the requirements for a Ph.D. degree from the University of Groningen by T.R.

Over the past three decades, the role of the ocean in the carbon cycle has been intensively studied, focusing on the food web structure and trophic interactions between the main functional groups of the pelagic food web inhabiting the upper ocean and on the production and remineralization of particulate (POC) and dissolved organic carbon (DOC) (Buesseler 1998; Hansell 2002). A large dataset on phytoplankton organic carbon production and the export flux of carbon from the euphotic layer to the open ocean seafloor has been acquired mainly via determining bulk POC and DOC concentrations in the meso- and bathypelagic layers and by sediment trap studies. Based on the decreasing POC and DOC concentrations with depth, the carbon utilization of the meso- and bathypelagic realm has been estimated and modeled (Hopkinson and Vallino 2005).

The meso- and bathypelagic realm comprises ~75% of the volume of the global ocean; however, little is known about the microbial activity below 200-m depth because of the scarcity of direct rate measurements. Generally, these deep water layers are considered to support only limited microbial activity. This is deduced mainly from the refractory nature of the bathypelagic dissolved organic matter (DOM) pool with an average age of ~6,000 yr (Bauer et al. 1992) and the low temperature at these depths (~2–4°C) retarding metabolic rates. In concert, these two characteristic features of the deep sea led to the commonly accepted view that bathypelagic microbial activity approaches zero.

Prokaryotes are, however, numerous throughout the ocean although prokaryotic abundance typically declines by two orders of magnitude from the surface to the deep oceanic waters (Patching and Eardly 1997; Nagata et al. 2000). Furthermore, it has been recognized that prokaryotes, notably bacteria, play a key role in the decomposition of nonliving organic particles in the surface layers (Ducklow and Carlson 1992) and in mesopelagic waters (Cho and Azam 1988; Karl et al. 1988). The latter two studies presented evidence that POC concentrations decrease with depth more rapidly than one would deduce from bacterial activity measurements. This suggests that particle-associated bacteria solubilize more POC to DOC than they utilize. This hypothesis has been coined the "particle decomposition paradox" (Karl et al. 1988). One cannot rule out, however, that mesopelagic zooplankton are consuming part of this POC pool and thus account for the difference between mesopelagic bacterial carbon demand and the decrease in POC concentration with depth (Banse 1990).

Bacterial carbon demand and remineralization rates are often deduced from bacterial production measurements, calculating respiration from an average bacterial growth yield of 20–30% (Nagata et al. 2000; Ducklow et al. 2002). Thus, the major fraction of the carbon flow mediated by heterotrophic bacteria, i.e., respiration, is deduced from measurements of a minor fraction, i.e., organic carbon production. Recently, however, oceanic respiration has received considerable attention because it has been recognized as one of the major, albeit poorly constrained, components of the carbon flux in the biosphere (Del Giorgio et al. 1997; Williams 1998). Model estimates suggest that dark ocean respiration might be higher than hitherto assumed (Del Giorgio and Duarte 2002). A higher dark ocean respiration rate than predicted from POC export can only be resolved if fluxes of DOC are much more important than assumed thus far, or if respiration of the dark ocean has been grossly underestimated. There is evidence that DOC accumulating in the euphotic layer during the production period is exported into the mesopelagic realm during winter overturning of the water column (Carlson et al. 1994). The magnitude to which this occurs on a large scale in the open ocean is still unknown and most of the exported DOC is probably respired in the upper mesopelagic zone (Arístegui et al. 2002).

For the subtropical northeast Atlantic and the Gulf of Mexico, mean mesopelagic respiration amounted to 0.2 ± 0.1 mmol O_2 m^{-3} d^{-1} and 0.9 ± 0.6 mmol O_2 m^{-3} d^{-1}, respectively (Biddanda and Benner 1997; Arístegui et al. 2005). The few studies on dark ocean respiration rates report mainly potential rates derived from measurements of the activity of the electron transport system (ETS) (Packard et al. 1988; Arístegui et al. 2005). Indirectly, dark ocean respiration rates can be obtained from tracer studies (Feely et al. 2004) and POC fluxes estimated from sediment trap deployments (Antia et al. 2001).

It has been shown recently that the global ocean's interior harbors both Bacteria and Archaea (Karner et al. 2001; Herndl et al. 2005) with both groups of prokaryotes incorporating leucine. However, Archaea also incorporate inorganic carbon and dominate the total prokaryotic abundance in the meso- and bathypelagic realm of the North Atlantic (Herndl et al. 2005). Thus, the measured leucine incorporation of deep water prokaryotes is a measure of prokaryotic biomass production rather than being restricted to bacterial biomass synthesis only. Therefore, the term "prokaryotic production" is more appropriate than the commonly used term "bacterial production." Likewise, the term "prokaryotic respiration" is used in this paper because Archaea dominate prokaryotic abundance in the deep waters of the North Atlantic, although it is unknown at present to what extent Archaea actually contribute to the oxygen consumption of the deep-water prokaryotic community.

The aim of this study was to assess prokaryotic respiration and production in the dark ocean, following the eastern and western branches of the North Atlantic Deep Water (NADW) from its origin over 30–50 years of its progression in the oceanic conveyor belt system. We measured, along with other basic physicochemical parameters, prokaryotic production and respiration, because prokaryotes are the main drivers of carbon cycling in the dark ocean. Specifically, we focused on the major water masses of the North Atlantic down to a depth of ~4,000 m. Generally, we found a more active prokaryotic community than expected based on the few published reports on meso- and bathypelagic bacterial activity.

Methods

Study site and sampling—The eastern and western branches of the NADW were followed with the R/V

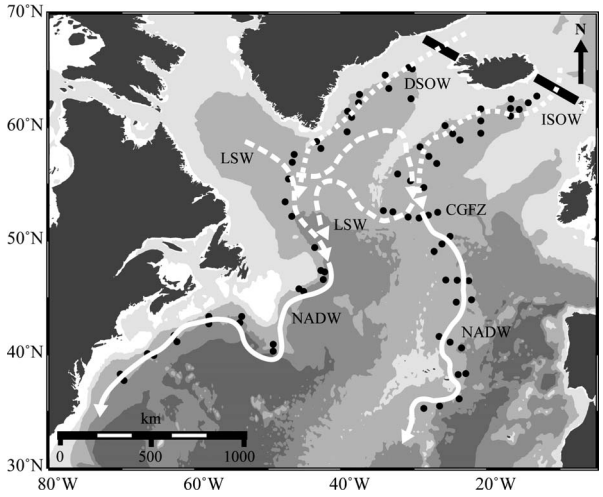

Fig. 1. Map of the study area in the North Atlantic. Dots indicate the individual stations occupied during TRANSAT-I (eastern basin; Sep 02) and TRANSAT-II (western basin; May 03). Lines and arrows indicate the flow of the main water masses (for abbreviations of water masses, see Table 1). Filled black bars denote position of the Greenland–Iceland–Scotland Ridge; Charlie-Gibbs Fracture Zone (CGFZ).

Pelagia from near its source of origin in the Greenland–Iceland–Norwegian Sea over two stretches, each more than 4,000 km long and corresponding to 30–50 years of the NADW progression in the oceanic conveyor belt system (Fig. 1). The TRANSAT-I cruise (Sep 02) followed a track from 62.8°N, 13.1°W to 35.3°N, 28.6°W in the eastern basin and the TRANSAT-II cruise (May 03) from 62.5°N, 30.3°W to 37.7°N, 69.7°W in the western basin of the North Atlantic. In total, 42 stations were occupied during the TRANSAT-I and 36 stations during the TRANSAT-II cruise.

Water was collected with a conductivity-temperature-depth (CTD) rosette sampler holding 24 12-liter NOEX (no oxygen exchange) bottles. Samples were taken from the main water masses encountered during the two cruises and from ~100 m depth (thereafter termed subsurface layer [SSL]) and the oxygen minimum zone (O_2-min). The main water masses sampled were the Labrador Seawater (LSW), the Iceland–Scotland Overflow Water (ISOW), the NADW, and the Denmark Strait Overflow Water (DSOW). These specific water masses were identified based on their temperature and salinity characteristics (Table 1) and their oxygen concentrations, using a Seabird SBE43 oxygen sensor mounted on the CTD frame. From these water masses, raw seawater samples were collected for total organic carbon (TOC), prokaryotic abundance and production and ETS measurements.

For prokaryotic respiration assays, seawater was filtered over rinsed 0.6-μm polycarbonate filters (Millipore) to exclude nonprokaryotic particles. Prokaryotic abundance and production were also determined in this 0.6-μm-filtered seawater. Additional samples were taken to determine the relative contribution and activity of Bacteria and Archaea in the prokaryotic community using catalyzed reporter deposition fluorescence in situ hybridization combined with microautoradiography. Results of these measurements are reported elsewhere (see Herndl et al. 2005; Teira et al. 2006).

Prokaryotic abundance—Samples (1 cm^3) of unfiltered and 0.6-μm-filtered seawater were fixed with 37% 0.2-μm-filtered (Acrodisc, Gelman) formaldehyde (2% final concentration), stained with 0.5 μL of SYBR Green I (Molecular Probes) at room temperature in the dark for 15 min and subsequently analyzed on a FACSCalibur flow cytometer (BD Biosciences) (Lebaron et al. 1998). Counts were performed with the argon laser at 488 nm set at an energy output of 15 mW. Prokaryotic cells were enumerated according to their right-angle light scatter and green fluorescence measured at 530 nm. Prokaryotic carbon biomass was calculated assuming a carbon content of 10 fg C per cell, which seems more appropriate for deep-sea prokaryotes than the generally used 20 fg carbon per cell (Ducklow et al. 2002).

Prokaryotic production—Prokaryotic production in the unfiltered and 0.6-μm-filtered seawater was measured by ^{3}H-leucine incorporation (specific activity: 595.7×10^{10} Bq $mmol^{-1}$ for TRANSAT-I and 558.7×10^{10} Bq $mmol^{-1}$ for TRANSAT-II; final concentration 10 nmol L^{-1}). Two 10–40-mL samples and 1 blank were incubated in the dark. The blank was fixed with concentrated 0.2-μm-filtered formaldehyde (4% final concentration, v/v) 10 min prior to adding the tracer. After incubating the samples and the blank at in situ temperature for 4–12 h, depending on the expected activity, the samples were fixed with formaldehyde (4% final concentration), filtered onto 0.2-μm nitrocellulose filters (Millipore HA; 25 mm diameter) and rinsed twice with 5 mL ice-cold 5% trichloroacetic acid (Sigma Chemicals) for 5 min. The filters were dissolved in 1 mL ethylacetate, and after 10 min, 8 mL of scintillation cocktail (Insta-Gel Plus, Canberra Packard) was added. The radioactivity incorporated into cells was counted in a liquid scintillation counter (Model 1212, LKB Wallac). Leucine incorporated into prokaryotic biomass was converted to carbon production using the theoretical conversion factor of 3.1 kg C mol^{-1} leu assuming a twofold isotope dilution (Simon and Azam 1989).

Prokaryotic respiration—The 0.6-μm filtrate was collected in an acid-rinsed (10% HCl and three times with 0.6-μm-filtered sample water) glass flask and subsequently transferred to calibrated borosilicate glass BOD bottles with a nominal volume of 120 cm^3 using silicon tubing fixed to the spigot of the glass flask, overflowing the bottles with at least three times the BOD bottle volume. For the determination of the initial O_2 concentration (t_0), samples were fixed immediately with Winkler reagents and incubated together with the live samples in water baths in the dark at in situ temperature (±1°C) for 34–96 h when the incubations were terminated (t_1). Triplicate bottles were used for the determination of initial and final O_2 concentrations. All the glassware was washed with 10% HCl and thoroughly rinsed with Milli-Q water prior to use. Oxygen concentrations of the t_0 and t_1 bottles were

Table 1. Averaged water mass properties of selected physicochemical parameters in the eastern and western North Atlantic basin. Salinity* (Sal), temperature* (T), apparent oxygen utilization* (AOU), total organic carbon* (TOC), subsurface layer (SSL), oxygen minimum zone (O_2-min), Labrador Sea Water (LSW), Iceland–Scotland Overflow Water (ISOW), North Atlantic Deep Water (NADW), Denmark Strait Overflow Water (DSOW).

Basin	Water mass	Mean pressure ($\times 10^1$ kPa)	Range ($\times 10^1$ kPa)	Sal	T (°C)	AOU (μmol kg^{-1})	TOC (mmol m^{-3})
Eastern	SSL (n=35)	135	90–150	35.48	11.06	19.63	56.0
				(0.41)	(2.89)	(5.72)	(7.3)
	O_2-min (n=38)	725	350–1,030	35.15	7.09	76.08	53.3
				(0.19)	(1.77)	(14.05)	(8.2)
	LSW (n=39)	1,816	1,160–2,130	34.91	3.40	37.68	51.3
				(0.03)	(0.21)	(6.39)	(6.3)
	ISOW (n=23)	2,429	1,720–3,100	34.97	2.76	41.16	50.1
				(0.01)	(0.29)	(4.20)	(6.9)
	NADW (n=25)	2,839	2,540–3,300	34.95	2.98	56.78	49.4
				(0.01)	(0.07)	(8.97)	(4.4)
Western	SSL (n=33)	100	90–110	35.17	8.73	27.73	56.8
				(0.58)	(4.74)	(19.15)	(8.7)
	O_2-min (n=15)	402	180–740	35.08	7.91	103.13	52.9
				(0.21)	(2.39)	(35.27)	(12.3)
	LSW (n=32)	1,324	710–2,090	34.89	3.44	42.04	52.3
				(0.02)	(0.32)	(6.03)	(8.8)
	NADW (n=25)	2,537	1,980–3,250	34.92	2.97	54.19	49.6
				(0.02)	(0.19)	(5.49)	(8.1)
	DSOW (n=22)	3,061	1,220–3,870	34.89	1.95	48.84	54.4
				(0.02)	(0.42)	(8.98)	(7.3)

* Top numbers are averages of the water masses; numbers in parentheses are standard deviations of the mean; n denotes the total number of samples for each water mass.

measured spectrophotometrically in a single run (Pai et al. 1993) following the standard protocol for the determination of oxygen by Winkler titration (Carritt and Carpenter 1966). Measurements were done in a temperature-controlled laboratory container (set at 20°C) on a Hitachi U-3010 spectrophotometer with a four-digit readout, using a 1-cm flow-through cuvette of 360 μL volume. The samples were withdrawn from the BOD bottles with a peristaltic pump (Gilson Minipuls) pumping the sample through the cuvette of the spectrophotometer via Teflon tubing. To avoid loss of volatile iodine, the bottles were covered with parafilm and the lower end of the sampling tube was placed close to the bottom of the BOD bottle. To prevent a photochemical change in color of iodine because of ambient light, the bottles were covered with dark tubes during the analysis. The amount of total iodine was determined at a wavelength of 456 nm and calculated from the mean of six photometrical readings per sample taken within 3 min.

The spectrophotometer was calibrated using standard additions of potassium iodate (J.T. Baker ACS grade KIO_3) to BOD bottles filled with seawater and adding Winkler chemicals in reverse order. The spectrophotometer was zeroed against a seawater blank. The coefficient of variation between triplicate samples was on average 0.08% at 280 mmol O_2 m^{-3}. The final oxygen consumption rates were converted to carbon units using a respiratory quotient of 1.

Activity of the ETS—ETS determinations were carried out only during TRANSAT-II following the modifications of the tetrazolium reduction technique as described in Arístegui and Montero (1995). Some minor modifications of the method were made to increase its sensitivity. Briefly, about 10 liters of water was filtered through a Whatman GF/F filter (47-mm diameter). Filters were folded into cryovials and immediately stored in liquid nitrogen until analysis in the laboratory. Back in the laboratory, the filters with the collected material were homogenized in 2.5 mL phosphate buffer with a Teflon-glass tissue grinder at 0–4°C for 1.5 min. An 0.9-mL aliquot of the crude homogenate was incubated in duplicate with 0.5 mL of substrate solution and 0.35 mL of 2-(4-iodophenyl)-3-(4-nitrophenyl)-5-phenyltetrazolium chloride (INT) at 18°C for 20 min. The reaction was quenched by adding 0.25 mL of a mixture of formalin and phosphoric acid. The quenched reaction mixture was centrifuged at 4,000 × g at 4°C for 20 min and the absorbance of the particle-free solution measured in a Beckman DU-650 spectrophotometer at 490 and 750 nm wavelengths after the sample was adjusted to room temperature. Readings at 750 nm, to correct for turbidity, were always negligible. In addition to the samples, duplicate controls were run by replacing the crude extract by a clean Whatman GF/F filter homogenized in phosphate buffer. ETS activity was calculated using the equation given in Packard and Williams (1981):

$$\mathrm{ETS_{ASSAY}\ (mmol\ O_2\ m^{-3}\ h^{-1})} = \mathrm{H} \times \mathrm{S} \times (\mathrm{OD_{corr}})/ (1.42 \times \mathrm{V} \times \mathrm{f} \times \mathrm{t}/60) \times 22.4$$

where H is the volume of the homogenate (in mL), S is the volume of the quenched reaction mixture (in mL), OD_{corr} is the absorbance of the sample measured at 490 nm

wavelength and corrected for blank absorbance, V is the volume (in liters) of the seawater filtered through the Whatman GF/F filter, f is the volume of the homogenate used in the assay (in mL), t is the incubation time (in min), 60 converts minutes to hours, the factor 1.42 converts the INT-formazan formed to oxygen units (in μL) and 22.4 converts the μL to mmol. ETS activity was corrected to in situ temperature using the following equation:

$$ETS_{IN\ SITU} = ETS_{ASSAY} \times e^{(Ea/R \times (1/Tass - 1/Tis)}$$

where Ea is the Arrhenius activation energy (in kcal mol^{-1}), R is the gas constant, and Tass and Tis are the temperatures (in degrees Kelvin) in the assay and in situ, respectively. A calculated activation energy of 16 kcal mol^{-1} was used.

Apparent oxygen utilization—Apparent oxygen utilization (AOU) is calculated as the difference between the saturation oxygen concentration and the observed oxygen concentration. The saturated oxygen concentration in seawater is dependent on the potential temperature, salinity and pressure of the sampling location. AOU was derived with the software package Ocean Data View (R. Schlitzer, ODV 2005, http://www.awi-bremerhaven.de/GEO/ODV/) using the CTD measurements of our depth profiles.

Statistical tests—Wherever appropriate, statistical tests were performed with the Tukey honest significant difference test at a significance level of $p < 0.5$ unless stated otherwise. For significance analysis, data were $\log_{10}$ transformed to obtain heteroscedascity.

Results

General hydrography of the water masses—The average depth, salinity, and temperature of the major water masses of the eastern and western basin of the North Atlantic are given in Table 1 along with mean AOU and TOC concentration. Maximum AOU was found in the oxygen minimum zone (O_2-min). On average, AOU in the O_2-min zone was significantly higher in the western than in the eastern basin ($p < 0.01$, $n = 15$), whereas AOU in the LSW and NADW was similar in both basins (Table 1). The TOC concentrations in the water masses of the western basin were slightly more variable than those in the eastern basin (Table 1). Generally, the TOC concentrations followed the commonly reported decrease with depth. In the western basin, however, the DSOW (depth range: 1,200–3,900 m) exhibited TOC concentrations not significantly lower than those of the SSL ($p = 0.33$, $n = 22$) indicating that the DSOW is younger than the NADW fueled by DSOW further south (at 60°N; Table 1).

Prokaryotic abundance—In both the eastern and western basin, total prokaryotic abundance decreased exponentially with depth ($r^2 = 0.77$, $p < 0.0001$, $n = 151$ and $r^2 = 0.91$, $p < 0.0001$, $n = 124$, respectively; Fig. 2). Despite this commonly reported pattern, however, prokaryotic abundance was more closely related to the specific water masses than the overall exponential decline in abundance with depth would suggest. The major source waters of the NADW, the ISOW and the DSOW (see Fig. 1), clearly identifiable north of 60°N, supported a higher prokaryotic abundance than the NADW ($p < 0.01$, $n = 20$), reflecting the more recent formation of these two water masses. The ISOW also carried a considerable particle load because of its near-bottom flow over the Iceland–Scotland Ridge (data not shown). Thus, it is likely that the resuspended particles in the ISOW contributed to the higher prokaryotic abundance than subsequently detected in the NADW, which is well separated from the seafloor by the Lower Deep Water and the recirculating Antarctic Bottom Water south of 55°N.

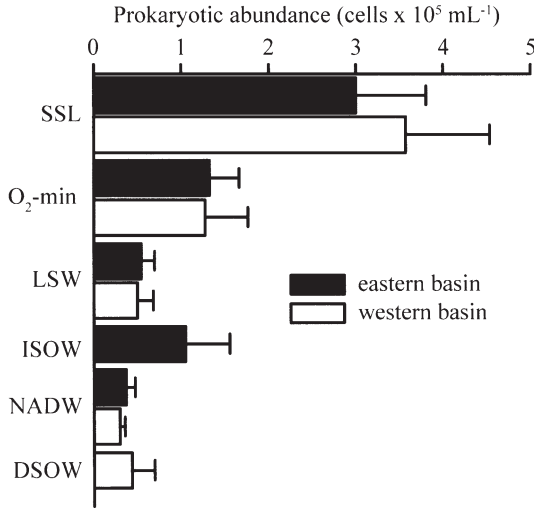

Fig. 2. Average prokaryotic abundance (cells $\times$ 10^5 mL^{-1}) in the different water masses of the eastern and western North Atlantic basin. Error bars show standard deviations.

Prokaryotic production (PKP) and cell-specific prokaryotic production—Similar to prokaryotic abundance, PKP decreased exponentially with depth ($r^2 = 0.63$, $p < 0.01$, $n = 180$ for the eastern basin and $r^2 = 0.65$, $p < 0.01$, $n = 139$ for the western basin) and was slightly higher (Student's t-test; $p < 0.01$, $n = 103$) in the western than in the eastern basin (Fig. 3a). In the eastern basin, PKP decreased from the SSL (9.2 $\pm$ 3.7 μmol C m^{-3} d^{-1}, $n = 31$) to the LSW (0.9 $\pm$ 0.6 μmol C m^{-3} d^{-1}, $n = 33$). PKP in the O_2-min layer between 350 and 1,000 m depth (2.1 $\pm$ 1.3 μmol C m^{-3} d^{-1}, $n = 33$) was identical to that in the ISOW (2.1 $\pm$ 1.3 μmol C m^{-3} d^{-1}, $n = 17$) found at a depth range of 1700–3100 m. Mean PKP in the eastern and western branches of the NADW was similar (1.1 $\pm$ 0.8 μmol C m^{-3} d^{-1}, $n = 22$, and 1.2 $\pm$ 0.8 μmol C m^{-3} d^{-1}, $n = 20$, respectively) and not significantly different ($p = 0.41$, $n = 20$) from the PKP in the DSOW (1.3 $\pm$ 0.8 μmol C m^{-3} d^{-1}, $n = 16$). PKP in the LSW of the western basin was, on average, twice as high ($p < 0.01$, $n = 26$) as in the eastern basin (1.9 $\pm$ 1.6 μmol C m^{-3} d^{-1} and 0.9 $\pm$ 0.6 μmol C m^{-3} d^{-1}, $n = 34$, respectively), reflecting its formation in the western basin.

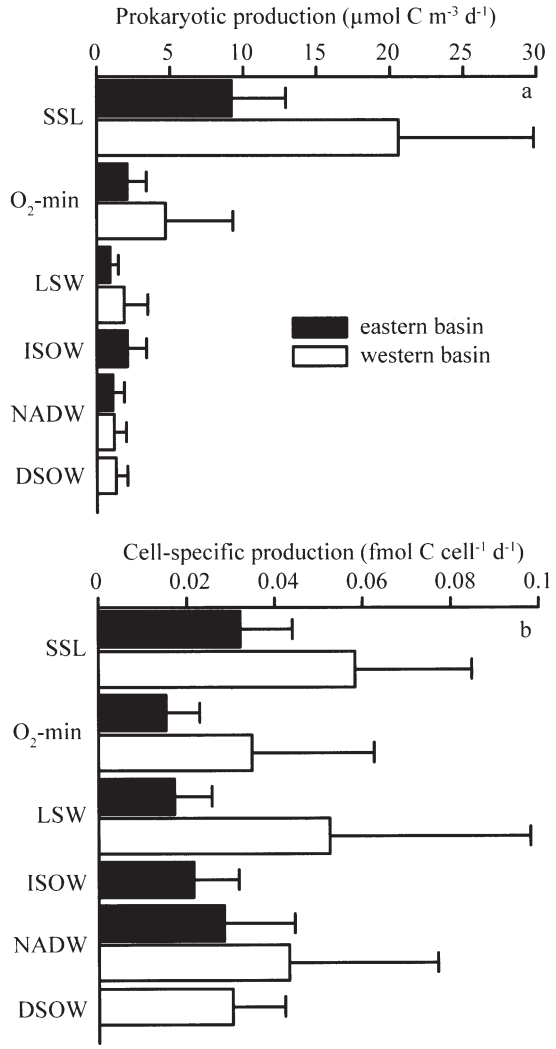

Fig. 3. (a) Prokaryotic production (μmol C m^{-3} d^{-1}) and (b) cell-specific prokaryotic production (fmol C cell^{-1} d^{-1}) in the different water masses of the eastern and western North Atlantic basin. Error bars show standard deviations; fmol = 10^{-15} mol.

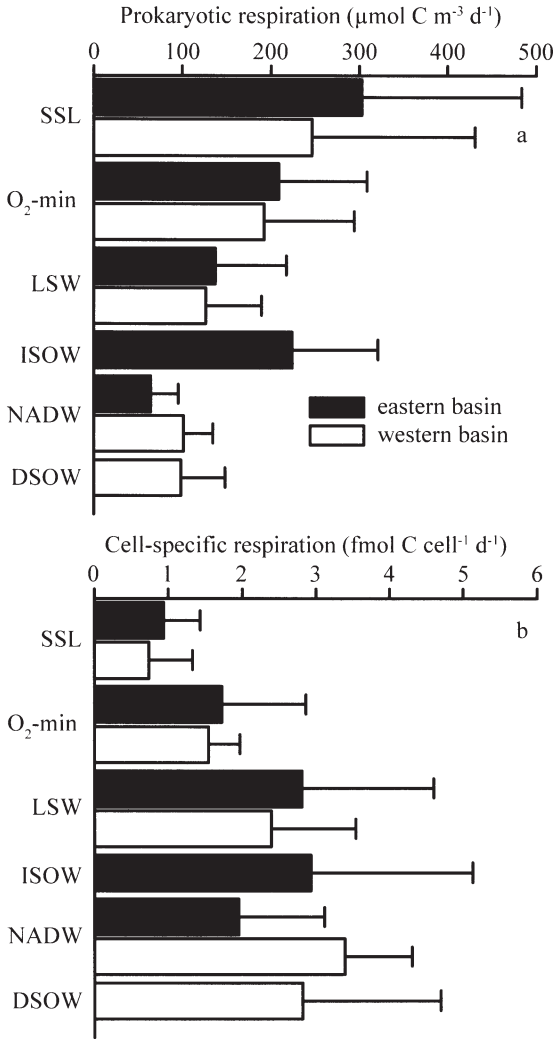

Fig. 4. (a) Prokaryotic respiration (μmol C m^{-3} d^{-1}) and (b) cell-specific prokaryotic respiration (fmol C cell^{-1} d^{-1}) in the different water masses of the eastern and western North Atlantic basin. Error bars show standard deviations; fmol = 10^{-15} mol.

Although both prokaryotic abundance and production decreased exponentially with depth, cell-specific prokaryotic production showed no systematic change (Fig. 3b). In the eastern North Atlantic basin, cell-specific PKP in the NADW ($28.4 \pm 16.0 \times 10^{-3}$ fmol C cell^{-1} d^{-1}, $n = 22$) was almost as high as in the SSL ($32.3 \pm 11.8 \times 10^{-3}$ fmol C cell^{-1} d^{-1}, $n = 31$) and about twice as high ($p < 0.01$, $n = 20$) as the cell-specific PKP in the O_2-min layer ($15.2 \pm 7.7 \times 10^{-3}$ fmol C cell^{-1} d^{-1}, $n = 31$) (Fig. 3b). In the western basin, cell-specific PKP ranged from $58.3 \pm 26.6 \times 10^{-3}$ fmol C cell^{-1} d^{-1} in the SSL to $30.3 \pm 11.9 \times 10^{-3}$ fmol C cell^{-1} d^{-1} in the DSOW (Fig. 3b) and was therefore overall 52% higher than the cell-specific PKP in the water masses of the eastern basin (Student's t-test; $p < 0.01$, $n = 101$) (Fig. 3b). Cell-specific PKP in the LSW of the western basin was 3 times higher than in the LSW of the eastern basin ($p < 0.01$, $n = 25$), again reflecting the more recent formation of the LSW in the western basin and older LSW in the eastern basin. In contrast, cell-specific PKP in the NADW of the western basin was only 34% higher ($p = 0.12$, $n = 20$) than in the eastern basin (Fig. 3b).

Bulk prokaryotic respiration (PKR) and cell-specific respiration rates measured via oxygen consumption—Only in the western basin, PKR decreased significantly with depth ($r^2 = 0.20$, $p < 0.01$, $n = 44$; Fig. 4a). In the eastern basin, PKR was not significantly different between the water masses ($p > 0.01$) with the exception of the NADW, in which PKR was about 21% of that in the SSL ($p < 0.01$) (Fig. 4a). It is noteworthy that PKR in the ISOW (224 ± 97 μmol C m^{-3} d^{-1}, $n = 6$) was as high as in the overlying O_2-min layer (208 ± 100 μmol C m^{-3} d^{-1}, $n = 10$; Fig. 4a) reflecting the pattern of the PKP (see Fig. 3a). In the western basin, PKR decreased from the SSL to the NADW and DSOW by 41% ($p < 0.01$ for both).

Cell-specific PKR, however, significantly increased from the SSL towards the deeper water masses ($r^2 = 0.30$, $p < 0.0001$ for the eastern and $r^2 = 0.50$, $p < 0.0001$ for the

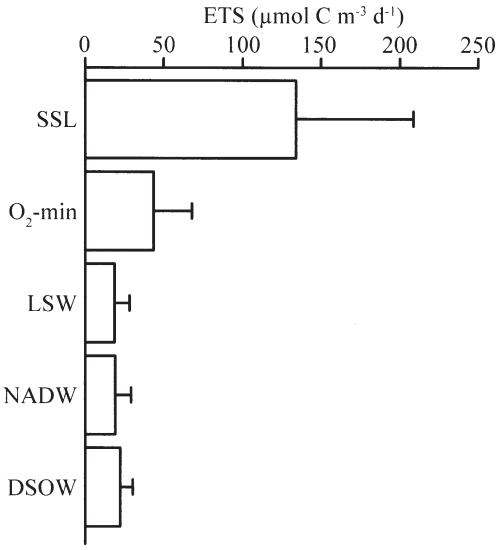

Fig. 5. Mean potential respiration rates measured via the electron transport system assay (ETS) in the different water masses of the western North Atlantic basin. Error bars show standard deviations.

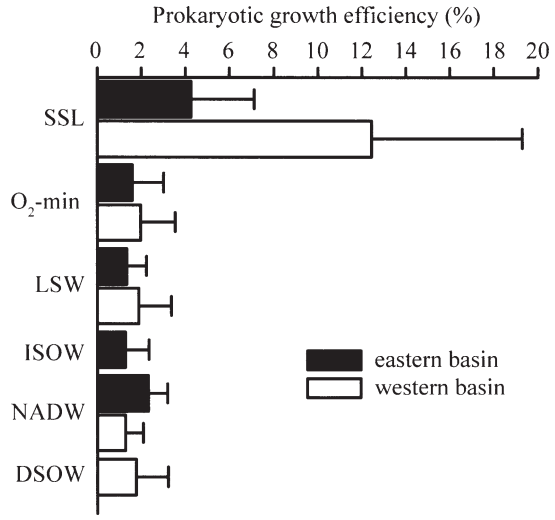

Fig. 6. Mean prokaryotic growth efficiency (%) based on oxygen consumption measurements in the different water masses of the eastern and western North Atlantic basin. Error bars show standard deviations.

western basin) in both basins (Fig. 4b). In contrast to cell-specific PKP, cell-specific PKR was not significantly different (Student's *t*-test; $p = 0.80$, $n = 44$) among the corresponding water masses of the eastern and western basin.

PKR estimated via ETS measurements—In the western basin of the North Atlantic, the respiratory activity of the deep water prokaryotic community was also determined via ETS measurements (Fig. 5). Whereas the respiration rates determined via O_2 consumption measurements decreased from the SSL to the NADW by 59% (Fig. 4a), potential respiration estimated via ETS measurements decreased by 85% (Fig. 5). Respiration rates estimated via ETS were rather similar for the different deep water masses (LSW, NADW, and DSOW) averaging 20.2 ± 9.0 µmol C m^{-3} d^{-1} ($n = 45$). Generally, PKR measured via O_2 consumption was ~45% and ~85% higher in the SSL and in the deeper water masses, respectively, than PKR estimated via ETS measurements (compare Fig. 4a and Fig. 5).

Prokaryotic growth efficiency (PGE)—For the SSL (depth range 90–150 m), the PGE in the eastern and western basin was, on average, 4 ± 3% ($n = 13$) and 12 ± 7% ($n = 11$), respectively (Fig. 6). Mean PGE for the water masses below the SSL was 2 ± 1% ($n = 56$, data from all the water masses below the SSL combined) for both North Atlantic basins. PGE was mainly determined by prokaryotic respiration and only weakly correlated with temperature ($r^2 = 0.13$, $n = 56$; data not shown).

Discussion

Prokaryotic production—Over the incubation period we used, no evidence was found that prokaryotic production in the 0.6-µm-filtered seawater was enhanced compared to unfiltered seawater, indicating that the filtration step did not alter the composition or quality of the DOM (Fig. 7). Our prokaryotic production estimates of the water masses of the deep North Atlantic are similar to the estimates of Nagata et al. (2000) for the deep North Pacific, the deep Arabian Sea (U.S. JGOFS Database) and a site in the southern North Atlantic (Patching and Eardly 1997). For the dark ocean, empirical conversion factors to translate prokaryotic uptake of radiolabeled tracers into cell production are not available. However, although the choice of the conversion factor is crucial for prokaryotic production estimates, its impact on the PGEs is comparatively small because of the high respiration compared to production.

Based on the prokaryotic production and biomass, we calculated the prokaryotic turnover time by dividing prokaryotic abundance by production (Kirchman 2002). In the eastern basin, mean prokaryotic turnover time ranged from 30 to 67 d. In the western basin, prokaryotic turnover times were more uniform throughout the different water masses and ranged from 17 to 39 d (Fig. 8). Our prokaryotic biomass estimates are based on flow cytometer counts of prokaryotic cells. Not all of these enumerated cells are alive, however; thus, the calculated turnover time is biased by the unknown fraction of inactive or dead cells. In a previous study, CARD-FISH targeting the 16S rRNA was used (Teira et al. 2004), which might serve as a proxy for active prokaryotes, because RNA rapidly degrades when cells decay. About 70% of all the DAPI-stainable cells were detected with fluorescently-labeled oligonucleotide probes, indicating that they contained sufficient RNA (Herndl et al. 2005). This 70% might be considered as a conservative estimate of the fraction of living prokaryotic cells. Calculating prokaryotic turnover times using the number of CARD-FISH stainable cells, we arrive at a turnover time of 7 d in the SSL and between 11 and 20 d in the water masses below, which is a decrease in turnover time of roughly 30–40% in all water masses. Thus,

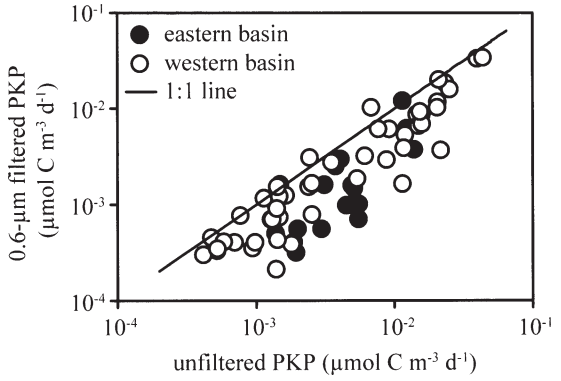

Fig. 7. Relationship of prokaryotic production (PKP; μmol C m^{-3} d^{-1}) measured in unfiltered and 0.6-μm-filtered seawater in the eastern and western basin. The line represents unity in rates of both fractions.

the fraction of deep water prokaryotes potentially metabolically active might be as high as in surface waters.

PKR—Although oxygen consumption measurements have adequate analytical precision, we are aware that they are problematic. Besides the often-cited bottle effect, the long incubation times required to obtain significant differences in the oxygen concentration between the start and the end of the incubation might pose problems. We addressed this potential problem by performing incubation experiments of 0.6-μm-filtered seawater from 400 m and 1,000 m depth for up to 192 h. The oxygen concentration decreased linearly, and the increase in prokaryotic abundance in an extra set of bottles was minimal over the maximum incubation period used to obtain the respiration rates (Fig. 9). Furthermore, the decrease in the oxygen concentration between t_0 and t_1 bottles was significant (Student's *t*-test; $p < 0.0001$, $n = 128$ for the eastern basin and $p < 0.02$, $n = 159$ for the western basin), and well

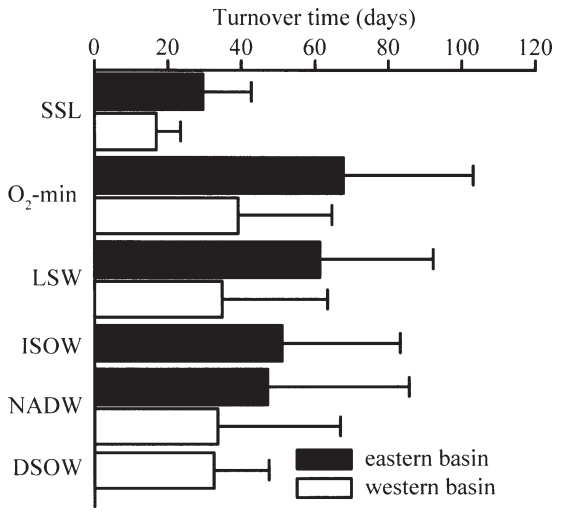

Fig. 8. Average turnover time (days) of the prokaryotic community in the different water masses of the eastern and western North Atlantic basin. Error bars show standard deviations.

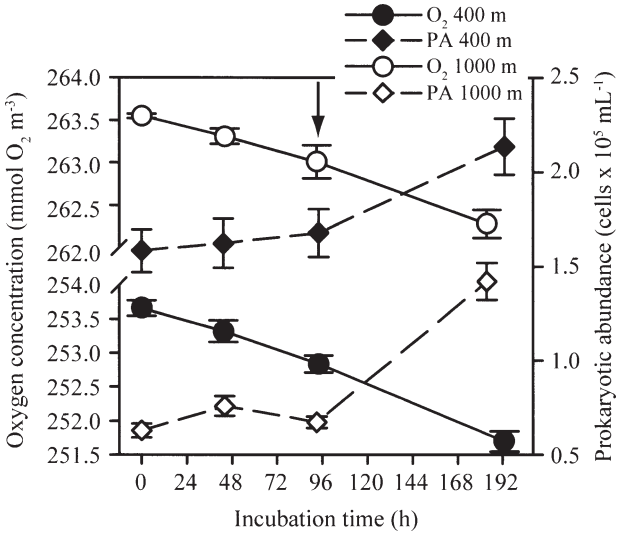

Fig. 9. Oxygen concentration (O_2; mmol O_2 m^{-3}) and prokaryotic abundance (PA; cells $\times$ 10^5 mL^{-1}) in 0.6-μm filtered seawater from 400 and 1,000 m. The arrow denotes the maximum used incubation time for the respiration measurements.

above the precision of the Winkler method (0.1–0.2 mmol O_2 m^{-3}). The respiratory quotient (RQ) to convert oxygen utilized to CO_2 produced varies between 0.7 and 1.3 depending on substrate composition (Biddanda and Benner 1997). In the absence of data on the nature of substrate respired, an RQ of 1 is applied assuming a mixed substrate composition. Considering that PGE is influenced mainly by PKR, the error in converting oxygen consumption to CO_2 (20–40%), is not as small as usually assumed. The uncertainty in this figure, however, does not change our main conclusions.

For the Gulf of Mexico, Biddanda and Benner (1997) reported oxygen consumption rates in the range of 1.7 to 0.9 mmol O_2 m^{-3} d^{-1} between 100 and 500 m depth. Prokaryotic respiration in the eastern and western basin of the North Atlantic was ~80% lower for similar depths (Fig. 4a); however, the temperature in the Gulf of Mexico is high (22–9°C in the top 100–500 m). Water mass transport time in combination with the AOU can be used to calculate oxygen utilization rates ($OUR = AOU/AGE_{water\ mass}$) (Suess 1980). Reported OURs for depths below 250 m are one to two orders of magnitude lower than our measured PKR (Suess 1980; Feely et al. 2004). Based on chlorofluorocarbon concentrations, the age of the NADW varies between 15 and 25 yr at the equator (Smethie et al. 2000; Fine et al. 2002), corresponding to spreading rates of the NADW and LSW of ~1–2 cm s^{-1}. Using this spreading rate and the AOU, mean OURs in the NADW and LSW amount to ~25% of our measured PKR in the eastern and ~30% in the western Atlantic basin.

PGE—PGEs in the range of 5–20% have been reported for surface waters of oligotrophic systems such as the Sargasso Sea, the central North Atlantic, and the Mediterranean Sea (Del Giorgio and Cole 2000 and references therein). Our calculated PGEs for the water masses of the

North Atlantic's interior are similar to the estimates of Griffith et al. (1990) for the outer shelf off Georgia (U.S.A.). For various shelf regions, Pomeroy et al. (1994) presented bacterial production and respiration data from near-surface waters. Assuming the conversion factors used in our study (3.1 kg C mol^{-1} leu; RQ = 1), the calculated PGEs ranged from 0.6–1.6% and were thus at the lower end of our deep water PGEs. Even lower PGEs of 0.01% were reported from the DYFAMED station in the Mediterranean Sea (Lemée et al. 2002). Thus, our PGEs obtained for the deep North Atlantic water masses are within the range reported for oligotrophic near-surface waters. For the mesopelagic realm of the Canary region of the North Atlantic, however, higher PGEs (13–18%) have been reported, likely caused by POC input via lateral advection from the African upwelling (Arístegui et al. 2005).

Growth efficiencies based on ETS measurements—ETS measurements should provide the upper limit of possible respiration rates (Packard and Williams 1981). The relation between enzymatic INT reduction and oxygen consumption, however, has not yet been firmly established. Commonly, a respiration : ETS ratio (R : ETS) of 0.086 is used, derived from batch culture experiments (Christensen et al. 1980). The assumed error for this conversion is ~30% (Packard et al. 1988). Using our measured ETS rates (Fig. 5) and applying the above R : ETS ratio to calculate PGEs, we obtain unrealistically high PGEs ranging between 40 and 66% for the SSL to the NADW of the western Atlantic basin. Recently, an eight-times-higher R : ETS ratio was calculated for the mesopelagic realm based on oxygen consumption and ETS measurements in the subtropical North Atlantic (Arístegui et al. 2005). Using our concurrently measured oxygen consumption (Fig. 4a) and ETS measurements (Fig. 5), we obtain an average R : ETS ratio of 5.3 over all the water masses (data not shown), which is 2 orders of magnitude higher than the R : ETS ratio obtained for bacteria in batch cultures. Thus, it seems that R : ETS ratios derived from batch cultures with high nutrient availability are of limited value for in situ studies.

Prokaryotic organic carbon demand (PCD) versus POC flux—It is generally assumed that POC exported from the euphotic layer is the main carbon source for the dark ocean and that DOC solubilized from POC provides the substrate for deep water prokaryotic plankton (Cho and Azam 1988; Karl et al. 1988). Calculating the PCD from the measured prokaryotic production and respiration (PCD = PKP + PKR) integrated over the water column, we arrive at a mean PCD of 436 mmol C m^{-2} d^{-1} averaged over both basins of the North Atlantic. To compare our mean PCD with the carbon flux into the dark ocean, we use the model of Antia et al. (2001), which is based on surface primary production and POC flux data ranging from the oligotrophic North Atlantic gyre to the subpolar region. The equation of Antia et al. (2001) is:

$$\text{POC-flux (mmol C m}^{-2}\text{ d}^{-1}) = 0.1 \times \text{PP}^{1.77} \times z^{-0.68}$$

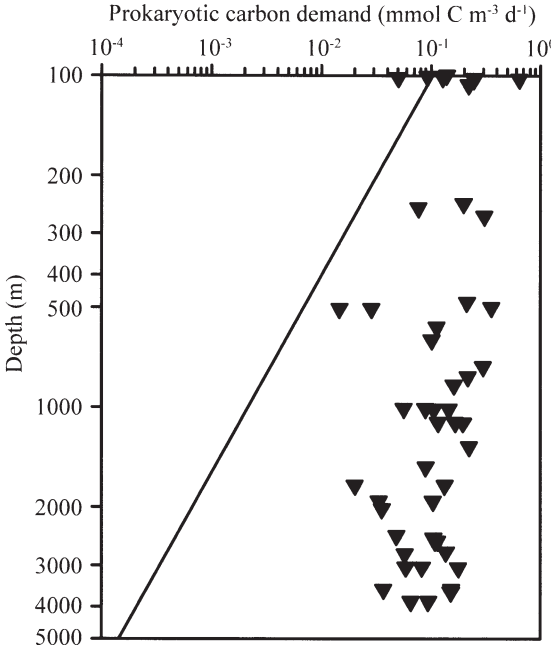

Fig. 10. Comparison of the prokaryotic carbon demand (PCD) and the availability of sinking POC in the western North Atlantic basin. The line represents the concentration of POC derived from surface primary production based on the POC flux model of Antia et al. (2001) assuming a primary production of 100 mmol C m^{-2} d^{-1} (see text). PCD was calculated using measured prokaryotic production and respiration (PCD = PKP + PKR).

where PP is the primary production (in mmol C m^{-2} d^{-1}) and z is the depth in m. The surface layer–derived POC arriving at a specific depth can thus be calculated from the above equation and is described by

$$\text{POC-available at z (mmol C m}^{-3}\text{ d}^{-1}) = 0.068 \times \text{PP}^{1.77} \times z^{-1.68}$$

For comparison with our PCD values, we assume a primary production of 100 mmol C m^{-2} d^{-1} reported from the North Atlantic Bloom Experiment (NABE) (Ducklow et al. 2002) and a decline in POC supply with depth following the above transformed equation. Clearly, our PCD values are higher than the POC supply at any given depth if a surface primary production of 100 mmol C m^{-2} d^{-1} is assumed (Fig. 10). In order to meet the PCD at greater depth, a primary production two orders of magnitude higher than that obtained during the NABE would be required. Particulate primary production measures taken during NABE are estimates of net primary production (Chipman et al. 1993) and thus might be substantially lower (60–70%) than gross primary production (Robinson et al. 2002). Thus, even a substantially higher gross primary production would be too low to account for the imbalance between PCD and organic carbon input into the dark ocean. Net heterotrophy in the North Atlantic surface waters, however, might be maintained via import of organic matter and

the unique thermohaline circulation pattern, whereas prokaryotic metabolism in deep waters acts as a trap for subducted organic matter (Hansell et al. 2004). One possible explanation of this apparent paradox is the different time scale over which the two data sets have been obtained. Whereas the POC flux data are derived from sediment trap studies, thus integrating over time spans of up to one year, the PCD values are based on snapshot measurements of production and respiration.

It is well known that sediment traps preferentially collect fast-sinking small particles and that slowly-sinking or buoyant large marine snow-type particles are underrepresented in sediment traps (Honjo et al. 1984; Asper 1987). Even in water samples collected with conventional sampling bottles, large aggregates are underrepresented because the largely very fragile aggregates are dispersed by the sampling procedure (Asper 1987). Nagata et al. (2000) found a direct relation between POC flux and bacterial carbon demand in the deep North Pacific. In the Arabian Sea, however, a similar relation was not detectable (Hansell and Ducklow 2003). Consequently, additional mechanisms of substrate and energy supply were proposed. A reassessment of the PCD (calculated from a PGE of 15%) in the Lagrangian NABE study revealed that the carbon flux including measured particulate primary production and estimated phytoplankton exudation would cover only ~70% of the PCD in the euphotic zone (Ducklow et al. 2002).

Based on $\Delta^{14}C$ measurements, Bauer et al. (2002) calculated that the concentrations of POC and DOC in the deep central gyres of the North West Atlantic are maintained via the relatively large lateral input from ocean margins rather than from recent surface production. The vertical diffusive flux of DOC in the Middle Atlantic Bight has been estimated to be on the order of 0.2 mmol C m^{-2} d^{-1} (Guo et al. 1995) and fluxes of ~3 mmol C m^{-2} d^{-1} via downwelling of DOC (Carlson et al. 1994) might also fuel deep water prokaryotic activity. Also, it has been shown that the labile fraction of the DOM pool exported from the euphotic zone is rich in carbon (Hopkinson and Vallino 2005). The relationship between the decrease in DOC concentrations and dark ocean respiration estimated from apparent oxygen utilization suggests, however, that only between 10% and 20% of the carbon demand in the deeper water layers is fueled by DOC (Arístegui et al. 2002).

Cell-specific production and respiration rates—In calculating cell-specific rates, we are aware of the uncertainties associated with the presence of nonviable cells. This would of course only give rise to an underestimation of the rates. In the deep water masses, cell-specific production amounted to 50–90% of that for surface waters (Fig. 3b). Similarly, biomass-specific rates of RNA and DNA synthesis by microorganisms in the meso- and bathypelagic regions suggest that microbial community growth is relatively uniform throughout the water column (Karl and Winn 1984). The respiration rates on a per-cell basis (Fig. 4b) are in the range of 1–5 fmol C $cell^{-1}$ d^{-1}, similar to those reported by Blight et al. (1995) for surface bacterioplankton. However, with the generally assumed decrease with depth of the particulate organic matter rain, our rates of cell-specific production and respiration cannot be explained. Remarkably, the increase of cell-specific respiration with depth (Fig. 4b) was also accompanied by an increasing percentage of cells with a high DNA content as measured by flow cytometry (data not shown). High-DNA-content bacteria are assumed to be more active than low-DNA-content bacteria (Gasol et al. 1999). The observed general decrease of growth efficiency with depth is a consequence of the increase in prokaryotic respiration, not of the decrease in prokaryotic production. This might suggest that the more refractory organic matter in the dark ocean gives rise to extra metabolic demands. However, this remains to be shown.

Decompression of the samples retrieved from greater depth prior to measuring production and respiration might have led to a stimulation of prokaryotic activity. Because we obtained prokaryotic growth yields of ~2% for the deep-water masses (Fig. 6), this would indicate that both production and respiration were stimulated similarly. Grossly over- or underestimating only one of these two parameters would have resulted in unrealistic prokaryotic growth yields. Whether decompression leads to a stimulation or inhibition of prokaryotic activity, however, is unclear. There is evidence that deep water prokaryotic activity is overestimated if measured under decompressed conditions (Jannasch and Wirsen 1982). However, other authors report inhibition of prokaryotic activity because of decompression (Tamburini et al. 2003).

The finding that dark-ocean PCD exceeds the supply from surface waters has also been reported by others (Smith and Kaufmann 1999; Del Giorgio and Duarte 2002; Ducklow et al. 2002) and resolving this discrepancy is a major contemporary challenge. This large discrepancy between prokaryotic carbon demand and carbon flux might be a result of methodological deficiencies in assessing organic carbon fluxes into the dark ocean and poorly constrained conversion factors needed to convert the rate measurements of leucine uptake into carbon. Prokaryotic production and respiration measurements of deep waters might also be biased because of depressurization upon retrieval of samples from the dark ocean. The current database on pressurized versus depressurized metabolic activity of deep-water prokaryotes is contradictory and needs to be resolved by obtaining prokaryotic activity measurements under realistic pressure conditions on a global scale. Despite all these uncertainties, we have shown that an active prokaryotic community exists in the dark ocean, and this adds weight to the emerging view that heterotrophic processes in the meso- and bathypelagic realm might play a major role in the biogeochemical cycles of the oceans.

References

Antia, A., and others. 2001. Basin-wide particulate carbon flux in the Atlantic Ocean: Regional export patterns and potential for atmospheric CO_2 sequestration. Glob. Biogeochem. Cycles **15:** 845–862.

Arístegui, J., C. M. Duarte, S. Agusti, M. D. Doval, X. A. Alvarez-Salgado, and D. A. Hansell. 2002. Dissolved organic carbon support of respiration in the dark ocean. Science **298:** 1976–1976.

———, ———, J. M. Gasol, and L. Alonso-Saez. 2005. Active mesopelagic prokaryotes support high respiration in the subtropical northeast Atlantic Ocean. Geophys. Res. Lett. **32:** [doi: 10.1029/2004GL021863].

———, and M. F. Montero. 1995. Plankton community respiration in Bransfield Strait (Antarctic Ocean) during austral spring. J. Plankton Res. **17:** 1647–1659.

Asper, V. L. 1987. Measuring the flux and sinking speed of marine snow aggregates. Deep-Sea Res. Part I **34:** 1–17.

Banse, K. 1990. New views on the degradation and disposition of organic particles as collected by sediment traps in the open sea. Deep-Sea Res. Part I **37:** 1177–1195.

Bauer, J. E., E. R. M. Druffel, D. M. Wolgast, and S. Griffin. 2002. Temporal and regional variability in sources and cycling of DOC and POC in the Northwest Atlantic continental shelf and slope. Deep-Sea Res. Part II **49:** 4387–4419.

———, P. M. Williams, and E. R. M. Druffel. 1992. C-14 Activity of dissolved organic carbon fractions in the north central Pacific and Sargasso Sea. Nature **357:** 667–670.

Biddanda, B., and R. Benner. 1997. Major contribution from mesopelagic plankton to heterotrophic metabolism in the upper ocean. Deep-Sea Res. Part I **44:** 2069–2085.

Blight, S. P., T. L. Bentley, D. Lefèvre, C. Robinson, R. Rodrigues, J. Rowlands, and P. J. l. B. Williams. 1995. Phasing of autotrophic and heterotrophic plankton metabolism in a temperate coastal ecosystem. Mar. Ecol. Prog. Ser. **128:** 61–75.

Buesseler, K. O. 1998. The decoupling of production and particulate export in the surface ocean. Glob. Biogeochem. Cycles **12:** 297–310.

Carlson, C. A., H. W. Ducklow, and A. F. Michaels. 1994. Annual flux of dissolved organic carbon from the euphotic zone in the northwestern Sargasso Sea. Nature **371:** 405–408.

Carritt, D. E., and J. H. Carpenter. 1966. Comparison and evaluation of currently employed modifications of Winkler method for determining dissolved oxygen in seawater—a NASCO Report. J. Mar. Res. **24:** 287–318.

Chipman, D. W., J. Marra, and T. Takahashi. 1993. Primary production at 47°N and 20°W in the North Atlantic ocean—a comparison between the C14 incubation method and the mixed layer carbon budget. Deep-Sea Res. Part II **40:** 151–169.

Cho, B. C., and F. Azam. 1988. Major role of bacteria in biogeochemical fluxes in the ocean's interior. Nature **332:** 441–443.

Christensen, J. P., T. G. Owens, A. H. Devol, and T. T. Packard. 1980. Respiration and physiological state in marine bacteria. Mar. Biol. **55:** 267–276.

Del Giorgio, P. A., and J. J. Cole. 2000. Bacterial energetics and growth efficiency, p. 289–325. *In* D. L. Kirchman [ed.], Microbial ecology of the oceans. Wiley-Liss.

———, ———, and A. Cimberis. 1997. Respiration rates of bacteria exceed phytoplankton in unproductive aquatic systems. Nature **385:** 148–151.

———, and C. M. Duarte. 2002. Respiration in the open ocean. Nature **420:** 379–384.

Ducklow, H. W., and C. A. Carlson. 1992. Oceanic bacterial production. Adv. Microb. Ecol. **12:** 113–181.

———, D. L. Kirchman, and T. R. Anderson. 2002. The magnitude of spring bacterial production in the North Atlantic Ocean. Limnol. Oceanogr. **47:** 1684–1693.

Feely, R. A., C. L. Sabine, R. Schlitzer, J. L. Bullister, S. Mecking, and D. Greeley. 2004. Oxygen utilization and organic carbon remineralization in the upper water column of the Pacific Ocean. J. Oceanogr. **60:** 45–52.

Fine, R. A., M. Rhein, and C. Andrié. 2002. Using a CFC effective age to estimate propagation and storage of climate anomalies in the deep western North Atlantic Ocean. Geophys. Res. Lett. **24:** 2227–2231.

Gasol, J. M., U. L. Zweifel, F. Peters, J. A. Fuhrman, and A. Hagström. 1999. Significance of size and nucleic acid content heterogeneity as measured by flow cytometry in natural planktonic bacteria. Appl. Environ. Microbiol. **65:** 4475–4483.

Griffith, P. C., D. J. Douglas, and S. C. Wainright. 1990. Metabolic activity of size-fractionated microbial plankton in estuarine, nearshore, and continental shelf waters of Georgia. Mar. Ecol. Prog. Ser. **59:** 263–270.

Guo, L., P. H. Santschi, and K. W. Warnken. 1995. Dynamics of dissolved organic carbon (DOC) in oceanic environments. Limnol. Oceanogr. **40:** 1392–1403.

Hansell, D. A. 2002. DOC in the global ocean carbon cycle, p. 685–715. *In* D. A. Hansell and C. A. Carlson [eds.], Biogeochemistry of marine dissolved organic matter. Academic.

———, and H. W. Ducklow. 2003. Bacterioplankton distribution and production in the bathypelagic ocean: Directly coupled to particulate organic carbon export? Limnol. Oceanogr. **48:** 150–156.

———, ———, A. M. Macdonald, and M. O. N. Baringer. 2004. Metabolic poise in the North Atlantic Ocean diagnosed from organic matter transports. Limnol. Oceanogr. **49:** 1084–1094.

Herndl, G. J., T. Reinthaler, E. Teira, H. van Aken, C. Veth, A. Pernthaler, and J. Pernthaler. 2005. Contribution of archaea to total prokaryotic production in the deep Atlantic ocean. Appl. Environ. Microbiol. **71:** 2303–2309.

Honjo, S., K. W. Doherty, Y. C. Agrawal, and V. L. Asper. 1984. Direct optical assessment of large amorphous aggregates (marine snow) in the deep ocean. Deep-Sea Res. Part I **31:** 67–76.

Hopkinson, C. S., and J. J. Vallino. 2005. Efficient export of carbon to the deep ocean through dissolved organic matter. Nature **433:** 142–145.

Jannasch, H. J., and C. O. Wirsen. 1982. Microbial activities in undecompressed microbial populations from the deep seawater samples. Appl. Environ. Microbiol. **43:** 1116–1124.

Karl, D. M., G. A. Knauer, and J. H. Martin. 1988. Downward flux of particulate organic matter in the ocean—a particle decomposition paradox. Nature **332:** 438–441.

———, and C. D. Winn. 1984. Adenine metabolism and nucleic acid synthesis: Applications to microbiological oceanography, p. 197–262. *In* J. E. Hobbie and P. J. l. B. Williams [eds.], Heterotrophic activity in the sea. Plenum.

Karner, M. B., E. F. Delong, and D. M. Karl. 2001. Archaeal dominance in the mesopelagic zone of the Pacific Ocean. Nature **409:** 507–510.

Kirchman, D. L. 2002. Calculation microbial growth rates from data on production and standing stocks. Mar. Ecol. Prog. Ser. **233:** 303–306.

Lebaron, P., N. Parthuisot, and P. Catala. 1998. Comparison of blue nucleic acid dyes for flow cytometric enumeration of bacteria in aquatic systems. Appl. Environ. Microbiol. **64:** 1725–1730.

Lemée, R., E. Rochelle-Newall, F. Van Wambeke, M.-D. Pizay, P. Rinaldi, and J.-P. Gattuso. 2002. Seasonal variation of bacterial production, respiration and growth efficiency in the open NW Mediterranean Sea. Aquat. Microb. Ecol. **29:** 227–237.

NAGATA, T., H. FUKUDA, R. FUKUDA, AND I. KOIKE. 2000. Bacterioplankton distribution and production in deep Pacific waters: Large-scale geographic variations and possible coupling with sinking particle fluxes. Limnol. Oceanogr. **45:** 426–435.

PACKARD, T. T., M. DENIS, M. RODIER, AND P. GARFIELD. 1988. Deep ocean metabolic CO_2 production—calculations from ETS activity. Deep-Sea Res. Part I **35:** 371–382.

———, AND P.J.L. B. WILLIAMS. 1981. Rates of respiratory oxygen-consumption and electron-transport in surface seawater from the Northwest Atlantic. Oceanol. Acta **4:** 351–358.

PAI, S.-C., G.-C. GONG, AND K.-K. LIU. 1993. Determination of dissolved oxygen in seawater by direct spectrophotometry of total iodine. Mar. Chem. **41:** 343–351.

PATCHING, J. W., AND D. EARDLY. 1997. Bacterial biomass and activity in the deep waters of the eastern Atlantic—evidence of a barophilic community. Deep-Sea Res. Part I **44:** 9–10.

POMEROY, L. R., J. E. SHELDON, AND W. M. SHELDON. 1994. Changes in bacterial numbers and leucine assimilation during estimations of microbial respiratory rates in seawater by the precision Winkler method. Appl. Environ. Microbiol. **60:** 328–332.

ROBINSON, C., P. SERRET, G. TILSTONE, E. TEIRA, M. V. ZUBKOV, A. P. REES, AND E. M. S. WOODWARD. 2002. Plankton respiration in the Eastern Atlantic Ocean. Deep-Sea Res. Part I **49:** 787–813.

SIMON, M., AND F. AZAM. 1989. Protein content and protein synthesis rates of planktonic marine bacteria. Mar. Ecol. Prog. Ser. **51:** 201–213.

SMETHIE, W. M., R. A. FINE, A. PUTZKA, AND E. P. JONES. 2000. Tracing the flow of North Atlantic Deep Water using chlorofluorocarbons. J. Geophys. Res.—Oceans **105:** 14297–14323.

SMITH, K. L., JR., AND R. S. KAUFMANN. 1999. Long-term discrepancy between food supply and demand in the deep eastern North Pacific. Science **284:** 1174–1177.

SUESS, E. 1980. Particulate organic carbon flux in the oceans—surface productivity and oxygen utilization. Nature **288:** 260–263.

TAMBURINI, C., J. GARCIN, AND A. BIANCHI. 2003. Role of deep-sea bacteria in organic matter mineralization and adaptation to hydrostatic pressure conditions in the NW Mediterranean Sea. Aquat. Microb. Ecol. **32:** 209–218.

TEIRA, E., T. REINTHALER, A. PERNTHALER, J. PERNTHALER, AND G. J. HERNDL. 2004. Combining catalyzed reporter deposition-fluorescence in situ hybridization and microautoradiography to detect substrate utilization by bacteria and archaea in the deep ocean. Appl. Environ. Microbiol. **70:** 4411–4414.

———, H. VAN AKEN, C. VETH, AND G. J. HERNDL. 2006. Archaeal uptake of enantiomeric amino acids in the meso- and bathypelagic waters of the North Atlantic. Limnol. Oceanogr. **51:** 60–69.

WILLIAMS, P. J. L. B. 1998. The balance of plankton respiration and photosynthesis in the open oceans. Nature **394:** 55–57.

Received: 30 May 2005
Accepted: 11 November 2005
Amended: 9 January 2006